Available online at www.sciencedirect.com
SCIENCE DIRECT®
Applied Surface Science 248 (2005) 484–491
applied surface science
www.elsevier.com/locate/apsusc

Laser generated soliton waveguides in photorefractive crystals

V.I. Vlad [a,*], E. Fazio [b], M. Bertolotti [b], A. Bosco [b], A. Petris [a]

[a] *Institute of Atomic Physics, NILPRP – Romanian Center of Excellence in Photonics and The Romanian Academy – CASP, Bucharest, Romania*
[b] *Università degli Studi di Roma "La Sapienza" and INFM, Roma, Italy*

Abstract

Non-linear photo-excited processes using the photorefractive effect are revisited with emphasis on spatial soliton generation in special laser beam propagation conditions. The soliton beams can create reversible or irreversible single-mode waveguides in the propagating materials. The important features are the 3D orientation and graded index profile matched to the laser fundamental mode. Bright spatial solitons are theoretically demonstrated and experimentally observed for the propagation of c.w. and pulsed femtosecond laser beams in photorefractive materials such as Bi_{12} SiO_{20} (BSO) and lithium niobate crystals. Applications in high coupling efficiency, adaptive optical interconnections and photonic crystal production are possible.

PACS: 42.65.T; 42.65.W; 42.65.H

Keywords: Solitons; Optical waveguides; Photorefractive crystals

1. Introduction

Spatial solitons with two-dimensional confinement have already been observed and studied in photorefractive materials [1–11]. Some widely available photorefractive materials show strong optical activity, which was considered for a long time as detrimental for spatial soliton formation and their stability. Recently, we have theoretically demonstrated and experimentally observed that, properly used, optical activity facilitates the creation of stable (2 + 1)D solitons in photorefractive crystals (PRC) [6–11]. The soliton is considered as a self-guided mode, as it writes a reversible or irreversible single-mode waveguide (WG) with a refractive index profile described by a $sech^2$ spatial dependence [1–3]. Consequently, a new concept of guiding light by light was developed and proved in different non-linear materials, including PRC [12–16].

In this paper, we are describing soliton solutions of the propagation equations and soliton polarisation evolution in PRC with optical activity, non-linear birefringence and absorption, which are fundamental for self-guiding [6–9] and provide control parameters for this process. The soliton WGs are considered

* Corresponding author.
E-mail address: vlad@ifin.nipne.ro (V.I. Vlad).

0169-4332/$ – see front matter © 2005 Elsevier B.V. All rights reserved.
doi:10.1016/j.apsusc.2005.03.098

together with some parameters, which ensure their stability. Soliton WGs can be obtained with low power lasers, may have 3D orientation in the material volume and a refractive index profile matched to the propagating beam. In order to show the serious advantages in the competition with the conventional (chemical) methods for light WGs writing, screening-photovoltaic bright solitons in lithium niobate (a common material for light WGs) and associated single-mode WGs were photo-induced [16,17]. We introduce a new concept: assisted light self-guiding (ALSEG) in low sensitive PRC by a sensitising background, which opens the possibility of soliton WG generation with laser wavelengths for which the common materials show poor photorefractive (PR) effects. First experiments, with self-guiding c.w. laser beams at 633 nm in BSO crystals assisted by a background of 514 nm wavelength proved the concept [14]. Here, we are presenting the development of ALSEG by self-guiding femtosecond–gaussian laser beams in lithium niobate crystals assisted by a c.w. background at 514 nm.

These soliton WGs may find important applications in modern optical communications providing high coupling efficiency and adaptive optical interconnections (source–fiber, fiber–fiber, fiber–chip).

2. Non-linear photo-excited processes in photorefractive crystals leading to soliton propagation

The photorefractive effect is a process, in which the local refractive index of an optical material, photoconductive and electro-optic, is changed, when illuminated by light with spatial variation of intensity. The PR effect is understood within the band transport model [1–4], where a PR material containing impurities can excite charges from donor sites into the conduction band, leaving a population of charges of opposite sign fixed in the excited sites. Such a population generates a local electric field, $E_{sc,}$ which may screen any externally applied static field, modifying consequently the material refractive index through the electro-optic Pockels effect:

$$\Delta n = \frac{1}{2} n_0^3 r_{\text{eff}} E_{\text{sc}}; \tag{1}$$

where r_{eff} is the effective linear electrooptic coefficient of the PR material. For a bell-shaped laser beam with intensity $I(x, z)$ illuminating the material, the steady state space charge field is [1–3]:

$$E_{\text{sc}} = \frac{E_0 - E_{\text{pv}} - (k_{\text{B}}T/e)\frac{\partial}{\partial x}[I(x,z)/I_{\text{B}}]}{1 + [I(x,z)/I_{\text{B}}]}, \tag{2}$$

where E_0 is the external electric field, E_{pv} is the electric field associated with the photovoltaic effect, K_{B} is the Boltzmann constant, T is the temperature, e is the elementary charge and I_{B} is the light background intensity. Thus, a uniform illumination washes out the refractive index distribution in the photorefractive material and resets it to the initial conditions.

If the carrier transport is dominated by drift, at high external electric fields, E_{sc} takes the form:

$$E_{\text{sc}} \approx \frac{E_0}{1 + I(x,z)/I_{\text{B}}} \tag{3}$$

depending nonlinearly on the ratio of the light and background intensities. This dependence is used in the generation of bright screening PR spatial solitons.

3. Soliton solutions of propagation equations in photorefractive crystals with optical activity, non-linear birefringence and absorption

Light propagation in a non-linear anisotropic material with optical activity and absorption can be described by the wave equation for the electric vector of the optical field, $\vec{E}$ [6–9]:

$$\Delta\vec{E}(\vec{r},t) - \frac{1}{c^2}\left[\hat{\varepsilon}\otimes\frac{\partial^2\vec{E}}{\partial t^2} + \frac{g}{k}\left(\vec{\nabla}\frac{\partial^2\vec{E}}{\partial t^2}\right)\right] - \frac{n_0}{c}\alpha\frac{\partial\vec{E}}{\partial t} = 0 \tag{4}$$

where c is the light velocity in vacuum, $\hat{\varepsilon}$ is the symmetric dielectric permittivity tensor of the anisotropic material, $g = 2\rho_0/k$ is the gyration constant, ρ_0 is the optical rotating power, k is the wave vector inside the material and α is the absorption coefficient.

In the steady state and drift dominated transport conditions, the change of the dielectric permittivity tensor of the PR crystal in function of light intensity is described by the equation:

$$\hat{\varepsilon} = [\vec{E}_0\hat{R}\cdot n_0^2]\left[1+\left(\frac{\vec{A}}{\sqrt{I_B}}\right)^2\right]^{-1}+\hat{\varepsilon}_0, \quad \text{where } \hat{\varepsilon}_0 = \begin{bmatrix} \varepsilon_{xx} & 0 \\ 0 & \varepsilon_{yy}\end{bmatrix}, \tag{5}$$

E_0 is the external electric field applied perpendicularly to the optical beams, $\hat{R}$ is the electro-optic tensor of the anisotropic material and ε_0 is the dielectric permittivity tensor in the dark. It is convenient to introduce *the non-linear birefringence coefficient*, c_1

$$c_1 = n_0^2 r_{\text{eff}} E_0 = (1/n_0^2)\Delta n, \tag{6}$$

and the *cylindrical coordinates scaled to* c_1:

$$\xi' = \rho\cos\varphi; \quad \eta' = \rho\sin\varphi; \quad \zeta' = \zeta = c_1 kz; \quad \rho = \sqrt{\xi'^2+\eta'^2} = \sqrt{c_1}k\sqrt{x^2+y^2}; \quad \varphi = \arctan\left(\frac{y}{x}\right) \tag{7}$$

At low light intensity levels, the intensity dependent factor from Eq. (5) can be linearly approximated as $(1 - I/I_B) = 1 - r\,(I/I_0)$, where I_0 is the maximum input intensity, and $r = I_0/I_B$. For an external electric field applied along [0 0 1] crystal direction, described by the parameter $\mu = 0$, the analytical solution of (4) for the optical field components was found as [6–9,15]:

The initial conditions lead to the relation, $w_0 \approx 6r/\pi^{3/2}$ and to small w_0, which are restrictive conditions for (2 + 1)D solitons. The soliton-like propagation is maintained in the presence of optical activity and absorption, with better confinement at higher external electric fields. The soliton width decreases by the external electric field increase (see Fig. 1b) and is given by:

$$w_s = \frac{\Delta\rho_t}{k\sqrt{n_0^2 r_{41} E_0}}. \tag{10}$$

At high light intensity levels, the intensity dependent factor in Eq. (5) is proportional to E_{sc} in the PR crystal and can be approximated by $[1 + (I/I_B)]^{-1} \sim (I/I_B)^{-1} = I_0/(rI)$. In this case the solutions become [6–9,15]:

$$\begin{bmatrix} A_x \\ A_y\end{bmatrix} = \sqrt{\frac{2I_B r}{\pi}}\gamma(\varphi,\zeta')\begin{bmatrix}\sin\theta & -\cos\theta \\ \cos\theta & \sin\theta\end{bmatrix} \times \begin{bmatrix}\psi_x(\rho_3) \\ e^{i\zeta'/2}\psi_y(\rho_3)\end{bmatrix} \tag{11}$$

with

$$\begin{bmatrix} A_x \\ A_y\end{bmatrix} = \sqrt{\frac{2I_B r}{\pi}}\gamma(\varphi,\zeta')\begin{bmatrix}\sin\theta & -\cos\theta \\ \cos\theta & \sin\theta\end{bmatrix}\begin{bmatrix}\exp\{-[\rho_1^2 w_0^2/(w_0^4+4\zeta'^2)]\}[\pi^2(w_0^4+4\zeta'^2)]^{-1/4} \\ e^{i\zeta'/2}\sqrt{2}ch^{-1}(\sqrt{2}\rho_1)\exp\{-[\rho_1^2/(w_0^2+4\zeta'^2/w_0^2)]\}\left[\pi^2(w_0^4+4\zeta'^2)\right]^{-1/4}\end{bmatrix} \tag{8}$$

defining a wave, which has a confined core and a weak diffraction part in both components. In (8), w_0 is the input Gaussian beam width, $\rho_1 = \sqrt{\frac{2r}{\pi}}\gamma(\varphi,z)\cdot\rho = \sqrt{\frac{2r}{\pi}}e^{-\alpha z/2}\left|\cos(1/2)(\varphi+gkz-\frac{\pi}{2}\right|^{-1}\cdot\rho = \rho/(\Delta\rho)_1$ and $(\Delta\rho)_1$ is the normalized beam width (for $r \ll 1$). The total intensity of this solitonic wave is (Fig. 1a):

$$I(\rho,\varphi,\zeta') = \frac{2}{\pi}I_B(r\gamma^2)[\psi_x^2+\psi_y^2] \approx \frac{2}{\pi^2 w_0^2}I_B(r\gamma^2) \times \exp\frac{-2\rho_1^2}{w_0^2}\left\lfloor 1+2\text{ch}^{-2}(\sqrt{2}\rho_1)\right\rfloor \tag{9}$$

$$\psi_x(\rho_3,\zeta') = \exp\{-[\rho_3^2 w_0^2/(w_0^4+4\zeta'^2)]\} \times [\pi^2(w_0^4+4\zeta'^2)]^{-1/4}$$

$$\psi_y(\rho_3,\zeta') = \pm\frac{\sqrt{2}\psi_x}{\text{ch}[\rho_3 - S_h^2/(1+S_h^2)]};$$

$$S_h^2 = \sqrt{\frac{\pi^2}{2w_0^4}(w_0^4+4\zeta'^2)\psi_y(0,\zeta') - 1} \tag{12}$$

The total intensity of this solitonic wave has the form shown in Fig. 1a and its expression is:

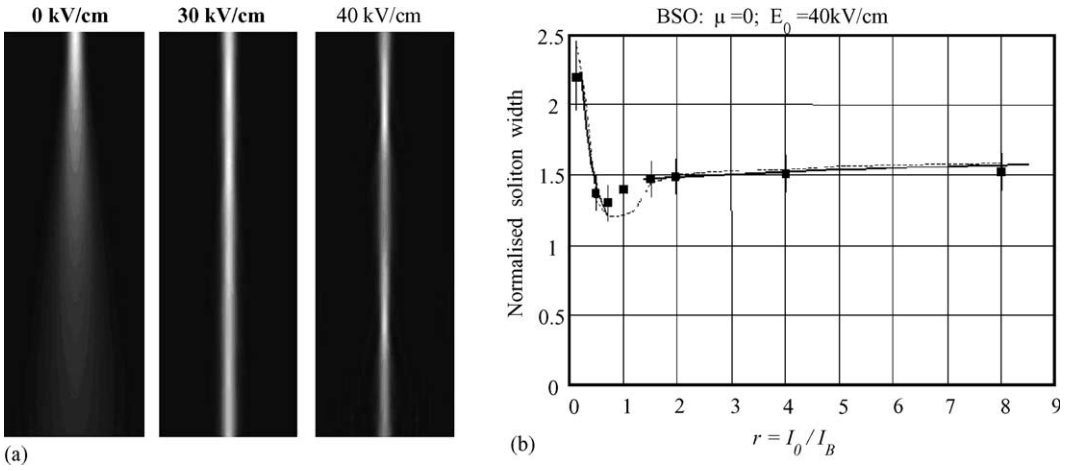

Fig. 1. (a) Propagation of a signal wave in BSO crystal along six diffraction lengths, for different external electric fields, demonstrating the soliton formation above 30 kV/cm. (b) Plot of the normalised experimental beam waist versus the signal/background intensity ratio r, at $E_0 = 40$ kV/cm; the analytical solutions are drawn with solid lines and the numerical solutions of Eq. (4) are shown by dashed lines [15].

$$I(\rho_3,\varphi,\zeta') = \frac{2}{\pi} I_B(r\gamma^2)[\psi_x^2+\psi_y^2] \approx \frac{2}{\pi^2 w_0^2} I_B(r\gamma^2) \times \exp\left(\frac{-2\rho_3^2}{w_0^2}\right) \lfloor 1 + 2\mathrm{ch}^{-2}(\sqrt{2}\rho_3) \rfloor \tag{13}$$

For an external electric field applied along the [1 1 0] crystal direction, described by the parameter $\mu = -1$, (2 + 1)D soliton propagation is possible [6–9,15].

The proportionality of the wave widths to $\sqrt{r}$, obtained by the analytical solutions, is in good agreement with the experimental findings (see Fig. 1b). The initial conditions introduce additional constraints: r is higher than 1, but close and $w_0^3 = r/\pi^{3/2}$.

The complete spatial soliton fields including the phases,

$$A_x = |A_x|e^{i\phi_x}, \quad A_y = |A_y|e^{i\phi_y}, \quad \phi = \phi_x - \phi_y \tag{14}$$

can be described by the polarization Stokes parameters S_0, S_1, S_2, S_3 [9–11,15]. Introducing the normalization of Stokes parameters to the soliton intensity, for representing on a Poincaré sphere with unit radius, one obtains:

$$\begin{aligned} S_0 &= 1 \\ S_1 &= -I_1 \cos 2\theta - I_2\left[\frac{\cos(\mu-1)\Delta nkz}{2n_0^2}\right]\sin 2\theta \\ S_2 &= I_1 \sin 2\theta - I_2\left[\frac{\cos(\mu-1)\Delta nkz}{2n_0^2}\right]\cos 2\theta \\ S_3 &= -I_2\left[\frac{\sin(\mu-1)\Delta nkz}{2n_0^2}\right] \end{aligned} \tag{15}$$

$$\text{where } I_1(\rho,z,\varphi) = \frac{\psi_x^2-\psi_y^2}{\psi_x^2+\psi_y^2},$$

$$I_2(\rho,z,\varphi) = \frac{2\psi_x\psi_y}{\psi_x^2+\psi_y^2}$$

$$\text{and } \theta = \frac{1}{2}\left(\varphi + 2\rho_0 z - \alpha z - \frac{\pi}{2}\right). \tag{16}$$

The Stokes parameters were analytically derived for low intensity, $r \ll 1$, and high intensity ratios, $r >\!\!> 1$, using the solutions from (9) and (13), for both mentioned crystal orientations i.e. $\mu = 0, -1$ [11]. Here, we present only the relations obtained for crystal orientation $\mu = 0$ and the high intensity ratios, used in our experiments. In Fig. 2, we have represented the polarization evolution of spatial solitons for BSO

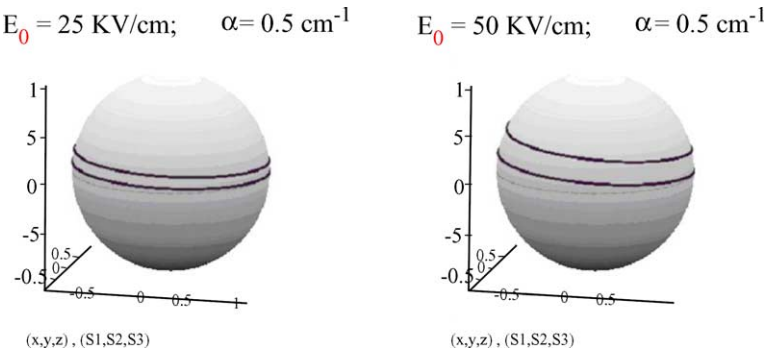

Fig. 2. Soliton polarization evolution on Poincaré sphere for $\mu = 0$, $r = 50$.

crystals, with the length $L = 8$ mm and with the following data:

$$n_0 = 2.615; \quad r_{41} = 5 \times 10^{-12} \frac{m}{V}; \quad \alpha = 50 m^{-1};$$

$$\rho_0 = 673.7 m^{-1}; \quad \lambda_0 = 0.5145 \times 10^{-6} m.$$

The experimental and analytical dependence of the soliton Stokes parameters on the external electric field is shown in the Fig. 3. The best fit with the theoretical curves corresponds to $r = 6.5$.

4. Soliton waveguides: optimum graded refractive index profile

Solitons are self-guided modes in their WGs. The self-consistency imposes on any self-guided mode to be a mode of the linear WG it induces.

The linear WGs with solitonic profiles, given by:

$$n^2(x) = n_\infty^2 + (n_0^2 - n_\infty^2)\mathrm{sech}^2 \frac{x}{\rho} \tag{17}$$

were treated by Snyder and Mitchell [13], where the amplitude of the fundamental mode of these WGs is given by:

$$A(x) = A_0 \mathrm{sech}^s \frac{x}{\rho}; \quad s = \frac{1}{2} \lfloor (1 + 4V^2)^{1/2} - 1 \rfloor . \tag{18}$$

The V parameter and the propagation constant are:

$$V = k\rho(n_0^2 - n_\infty^2)^{1/2}; \quad \beta^2 = (kn_\infty)^2 + \left(\frac{s}{\rho}\right)^2 \tag{19}$$

and the condition of a single-mode can be obtained as:

$$s \leq 1 \rightarrow V \leq \sqrt{2}. \tag{20}$$

The consistency with a power-law nonlinearity: $n_{\mathrm{NL}}^2 = n_\infty^2 + (\alpha I)^q$, in the low and high intensity cases, leads to [13]: $s \equiv 1/q \rightarrow V = \sqrt{1+q}/q$.

The condition for stable solitons is $q < 2$, which is compatible with our solutions.

5. Guiding of ultrafast pulsed beams

In order to emphasis the possibility and usefulness of soliton WGs, we have used the experimental set-up

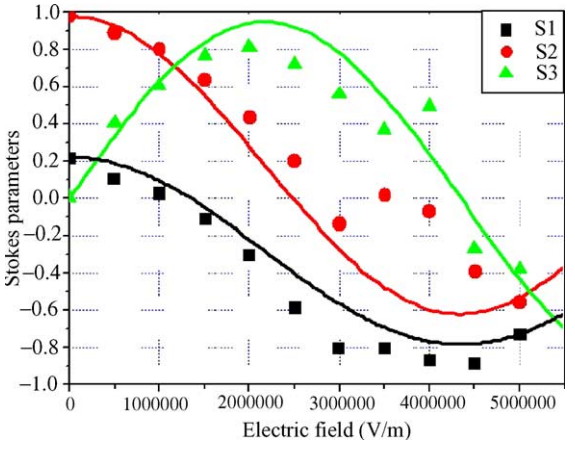

Fig. 3. The dependence of the soliton Stokes parameters on the external electric field, for a BSO crystal ($L = 8$ mm, $\alpha = 0.5$ cm^{-1} and orientation $\mu = 0$).

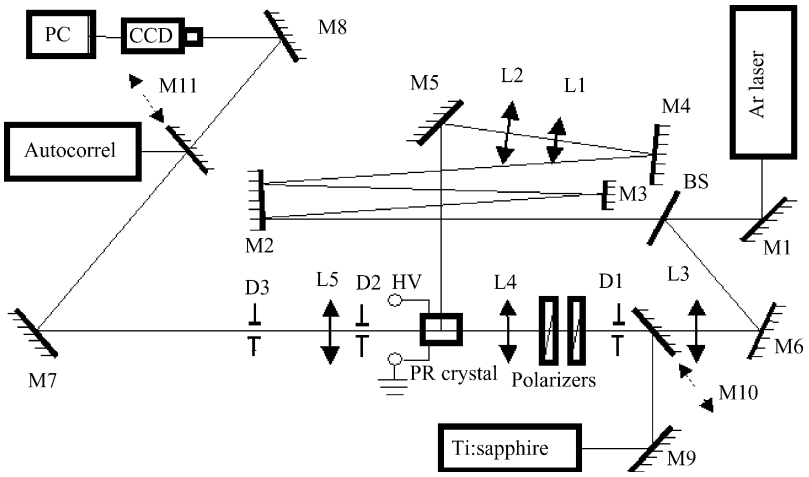

Fig. 4. Experimental set-up for generation soliton waveguides with a c.w. (Argon ion laser) and to study the propagation of femtosecond laser pulses through such waveguides.

shown in Fig. 4 for generation of soliton WGs in the common $LiNbO_3$ crystals and the propagation of femtosecond laser pulses through these waveguides. A laser beam from a c.w. Argon ion laser ($\lambda = 514$ nm), linearly polarized and a Gaussian transversal intensity distribution, was split into two beams for signal and background. The signal beam is focused to about 9 μm on the input face of the crystal of 5 mm thickness (~5 diffraction lengths). This beam propagated along the *z*-direction, orthogonally to the optical axis (*y*-direction). On the lithium niobate crystal a bias voltage is applied along the optical axis. The background beam, mutually incoherent to the signal beams, is expanded, spatially filtered and sent along the *x*-direction in the crystal. The crystal is immersed in a cell with insulating oil, placed on a stage that allows the fine adjustment of the crystal position for optimum coupling of the probe beam to the different soliton waveguides induced in the crystal. An imaging system is used to visualize the transversal shape of the signal beam at the entrance of the crystal and at its output face.

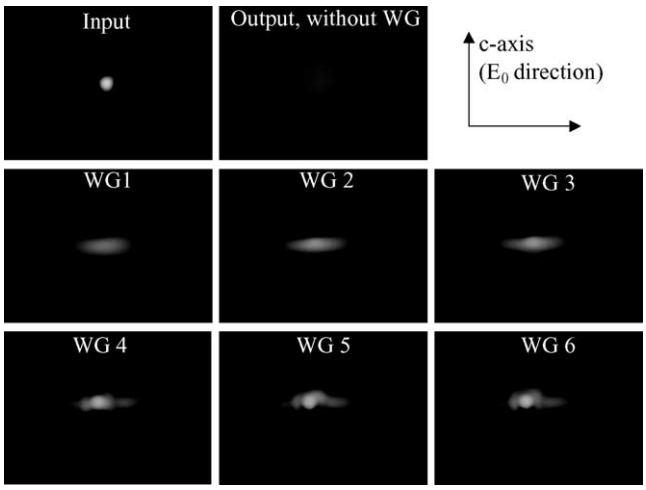

Fig. 5. Guiding femtosecond laser beams through soliton WGs created by a low power (10 μW) c.w. argon laser.

Table 1
Soliton waveguide dispersion for different exposure times to (fs) light pulses

Material	Average dispersion (fs/mm)
Crystal	9.86
WG1 15 min	10.00
WG2 30 min	10.18
WG3 30 min	10.15
WG4 60 min	10.75
WG5 90 min	10.55
WG6 90 min	10.71

The procedure for waveguide writing is described by Fazio et al. [16,17]. The soliton waveguide becomes cylindrical with circular sections at $E_0 = 35$ kV/cm and with a c.w. exposure for about 30 min. The temporal stability of the induced soliton waveguides was checked during time intervals up to 1 month by monitoring periodically their guiding properties with light with the same wavelength as used for writing. No change of the output profile of the beam transmitted through waveguide was observed.

The soliton waveguides induced in the lithium niobate crystal were tested by guiding 75 fs pulses generated by a mode-locked Ti:sapphire laser. Several waveguides induced for different recording times in the same $LiNbO_3$ crystal have been investigated i.e., WG 1, 15 min recording time; WG2 and WG 3, 30 min; WG 4, 60 min; WG 5 and WG 6, 90 min. The beam with 35 mW average power, injected in the waveguides, was vertically polarized. We compared the signal beam shape at the input with the beam shape at the output, within or outside the six different soliton waveguides. The results are shown in Fig. 5.

We measured the change of the pulse duration produced by the soliton waveguides by autocorrelation. The temporal profile of the pulses was fitted well by a sech^2 curve.

In Table 1, the dispersion of the pure material is compared to the dispersion of the pulses inside six soliton waveguides obtained with different exposure times. The waveguides introduce small changes of the linear dispersion (less than 10%).

6. Light self-guiding in low sensitive PRC assisted by a sensitising background

We have demonstrated a new concept: assisted light self-guiding in *low sensitive PRC* using a sensitising background (ALSEG). This concept was put in operation when the self-waveguiding of femtosecond pulses (at 800 nm) in a lithium niobate crystal (with very low PR effect at this wavelength) was demanded. We generated soliton waveguides using a Ti:sapphire

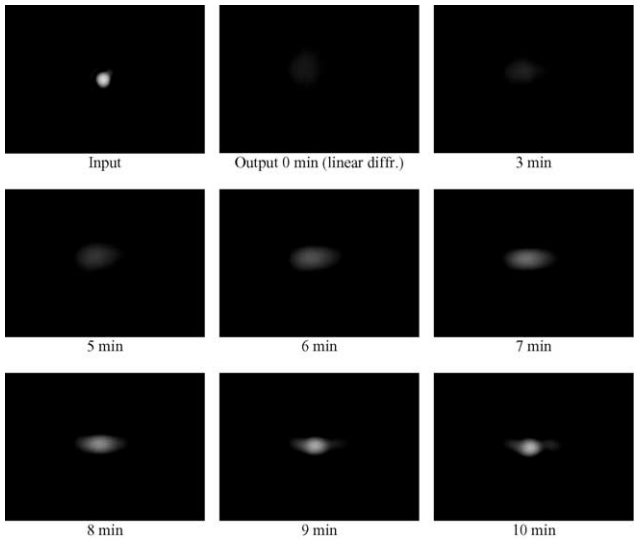

Fig. 6. Assisted light self-guiding in *low sensitive PRC* using a sensitising background (ALSEG) guiding of femtosecond laser pulses at 800 nm with a c.w. background at 514 nm.

laser beam (at 800 nm) as signal beam and the simultaneous illumination of the lithium niobate crystal with a sensitizing green cw background (provided by an Ar ion laser, at 514 nm).

In this case a perfect matching of the waveguide profile to the transmitted beam was achieved. The temporal evolution of the transversal shape of the femtosecond signal beam at the output of the crystal, for a bias of 35 kV/cm is shown in Fig. 6.

7. Conclusions

Analytical solutions of laser beam propagation equations in PRC show the occurrence of spatial solitons and the optimum conditions for guiding light by light. Solitons provide an easy and fast way for writing waveguides which are matched to the laser beam profiles. Solitons in PRC were shown to act as efficient waveguides for long times, which can be also erased on demand. Using a new concept, ALSEG, one can write waveguides in low sensitive PR materials. Bright spatial solitons were created in lithium niobate with both c.w. and femtosecond lasers. These soliton waveguides can be used in efficient coupling of laser diode to fibres, fibre to fibre, fibre to chip, as well as for splitters, routers, optical switches, reconfigurable interconnections and photonic crystals.

Acknowledgement

The authors acknowledge the support of the Bilateral Agreement between the Italian Ministry of Foreign Affairs and the Romanian Ministry of Education and Research project #36.

References

[1] M. Segev, B. Crosignani, A. Yariv, B. Fisher, Phys. Rev. Lett. 68 (1992) 923.
[2] G.C. Duree, J.L. Schultz, G.J. Salamo, M. Segev, A. Yariv, B. Crosignani, P. di Porto, E.J. Sharp, R.R. Neurgaonkar, Phys. Rev. Lett. 71 (1993) 533.
[3] D.N. Christodoulides, M.I. Carvalho, J. Opt. Soc. Am. B 12 (1995) 1628.
[4] S.R. Singh, D.N. Christodoulidis, J. Opt. Soc. Am. B 13 (1996) 719.
[5] W. Krolikowski, N. Akhmediev, D.R. Andersen, B. Luther-Davies, Opt. Commun. 132 (1996) 179.
[6] V.I. Vlad, V. Babin, M. Bertolotti, E. Fazio, M. Zitelli, Proc. Rom. Acad. A1 (1) (2000) 25;
V.I. Vlad, V. Babin, M. Bertolotti, E. Fazio, M. Zitelli, Proc. Rom. Acad. A1 (3) (2000).
[7] E. Fazio, F. Mariani, A. Funto, M. Zitelli, M. Bertolotti, V. Babin, V.I. Vlad, Proc. SPIE 4430 (2001) 411;
E. Fazio, F. Mariani, A. Funto, M. Zitelli, M. Bertolotti, V. Babin, V.I. Vlad, J. Optics A3 (2001) 466.
[8] E. Fazio, V. Babin, M. Bertolotti, V.I. Vlad, Phys. Rev. E 66 (2002) 016605.
[9] E. Fazio, W. Ramadan, A. Belardini, A. Bosco, M. Bertolotti, A. Petris, V.I. Vlad, Phys. Rev. E 67 (2003) 026611.
[10] E. Fazio, W. Ramadan, M. Bertolotti, A. Petris, V.I. Vlad, J. Optics A 5 (2003) S119.
[11] V.I. Vlad, A. Petris, V. Babin, E. Fazio, M. Bertolotti, Proc. SPIE 5581 (2004) 601.
[12] R. De La Fuente, A. Barthelemy, C. Froehly, Opt. Lett. 16 (1991) 793.
[13] A.W. Snyder, D.J. Mitchell, Opt. Lett. 18 (1993) 101–103.
[14] W. Ramadan, E. Fazio, A. Mascioletti, F. Inam, R. Rinaldi, A. Bosco, V.I. Vlad, A. Petris, M. Bertolotti, J. Optics A 6 (2003) S432–S436.
[15] V.I. Vlad, E. Fazio, M. Damzen, A. Petris, in: A. Peled (Ed.), Photoexcited Processes and Applications, Kluwer Academic Publishers, Amsterdam & NY, 2003, p. 57.
[16] E. Fazio, R. Renzi, R. Rinaldi, M. Bertolotti, M. Chauvet, W. Ramadan, A. Petris, V.I. Vlad, Appl. Phys. Lett. 13 (2004).
[17] E. Fazio, W. Ramadan, A. Petris, M. Chauvet, V.I. Vlad, M. Bertolotti, this issue.